CrossMark

Thermal oxidation-resistant GeO$_2$ ATR hollow waveguide based on NiCr capillary tube and its thermal effects

Xu Wang[1] · Lin Wang[1] · Xiaohong Fu[1] · Xuehui Lu[1] · Fangyu Yue[1] · Pingxiong Yang[1] · Xingzhong Yuan[3] · Chengbin Jing[1,2] · Junhao Chu[1,4]

Abstract

Transmission characteristics of a metallic tube GeO$_2$ ATR hollow waveguide degenerate due to metal thermal oxidation caused by transmission, coupling and misalignment losses. NiCr has intrinsic resistance to thermal oxidation and is often used in thermocouple heater. Thermogravimetric analysis shows that NiCr substrate tube material suffers no thermal oxidation with temperature up to 1100 °C. Thus, NiCr capillary tube is investigated for construction of a thermal oxidation-resistant GeO$_2$ ATR hollow fiber. A NiCr capillary tube GeO$_2$ ATR hollow fiber was fabricated based on liquid phase deposition. The fiber sample has a transmission attenuation of 0.25 dB/m when transmitting a 6-W CO$_2$ laser. Sample temperature distributions that originated from transmission loss and coupling loss are theoretically simulated and practically measured. Results confirm that the simulation can properly tell the influence of laser power losses on the fiber temperature and is further used to predict the maximum input power of the ATR fibers. To illustrate the thermal oxidation resistance of NiCr ATR hollow fiber, NiCr-based and stainless steel (SUS)-based ATR hollow fibers are directly irradiated by 6 W CO$_2$ laser. The SUS fiber input end became darkened. No obvious changes happened on NiCr fiber. Output beam profile and divergence angle are also taken to support the analysis. The NiCr capillary tube GeO$_2$ ATR hollow fiber is a good candidate for construction of durable GeO$_2$ ATR hollow fiber in high power applications.

1 Introduction

Infrared lasers have been widely used in military and domestic applications ranging from laser power delivery in medical surgery to thermal imaging and mid- or far-infrared spectroscopy [1–4]. In search for an ideal transmission system for infrared lasers, infrared hollow optical fibers such as

✉ Chengbin Jing
  cbjing@ee.ecnu.edu.cn

1   Key Laboratory of Polar Materials and Devices, Ministry of Education, Department of Electronic Engineering, East China Normal University, 500 Dongchuan Road, Shanghai 200241, China

2   Institute of Functional Materials, Department of Materials, School of Physics and Materials Science, East China Normal University, 500 Dongchuan Road, Shanghai 200241, China

3   Quality Department, Jiangsu Jiuxin Medical Technology Co., Ltd., Changzhou 213125, China

4   National Laboratory for Infrared Physics, Shanghai Institute of Technical Physics, Chinese Academy of Sciences, 500 Yu-tian Road, Shanghai 200083, China

hollow-core photonic band-gap fibers, leaky hollow fibers and attenuated total reflection (ATR) hollow fibers have been reported. ATR hollow fibers have received extensive attention for they have the same light-guiding mechanism as traditional solid-core ATR fibers and no end reflection. To construct an ATR hollow waveguide, the reflective layer of the waveguide is required to have a reflective index of $n_r < 1$ at the wavelength of interest. When light incident from the air ($n_r = 1$) to this reflective layer, the interface will exhibit total reflection behavior through which the light was transmitted. Sapphire, silicon carbide, germanate glass and GeO$_2$ show anomalous dispersion behavior around the wavelength of CO$_2$ laser, where they have reflective indexes less than 1. Single-crystal growth, melt-drawing fiber, sol–gel and chemical vapor deposition have been used to fabricate sapphire [5], germanate glass [6], germanium dioxide [7] and polycrystalline germanium dioxide [8] ATR hollow fibers for delivery of CO$_2$ laser radiations. A liquid phase deposition (LPD) process has been developed in our group for fabrication of GeO$_2$ ATR hollow fibers based on silica glass capillary tubes [9]. This method was further used to fabricate a series of metallic GeO$_2$ ATR hollow waveguides

based on Cu, Ni or stainless steel (SUS) [10–12]. Compared with silica glass, metallic GeO_2 ATR hollow waveguides are mechanically strong and can be easily connected to other metallic components by welding or using screw joints. GeO_2 film deposited on different substrate tubes has varied film quality, which influences the transmission characteristics. New materials should be investigated for construction of a GeO_2 ATR hollow waveguide. Although metallic tubes are robust compared to glass capillary tubes, they are prone to be oxidized in high temperature. An instant temperature rise may cause catastrophic damage to the metallic ATR waveguide. In previous study, transmission characteristics of the SUS hollow waveguide degenerate after several measurements and the input ends of the waveguides become darkened. This is the result of the inevitable laser power losses in hollow waveguide transmission, especially coupling and misalignment losses. The lost laser power transforms to heat and may cause severe heat damage to the hollow fiber. However, we believed that this disadvantage can be made up from the material point of view. Nichrome (NiCr), an alloy of nickel and chrome, is often used in devices where electric heating is required such as thermocouple heater. It is intrinsically stable in higher temperature environments. Thus, NiCr is a good candidate for constructing a thermal oxidation-resistant ATR hollow waveguide for CO_2 laser delivery. A method to simulate the influence of the lost power on waveguide temperature is needed to evaluate the practical thermal effects of metallic ATR hollow waveguides. Based on heat transmission model, Miyagi et al. have carried out a theoretical analysis to evaluate the power distribution and power handling capability of leaky waveguides [13]. With this method and taking transmission and structural difference into account, the thermal behaviors of the SUS ATR hollow fiber transmitting CO_2 laser were investigated theoretically and experimentally [14].

In this work, NiCr GeO_2 ATR hollow waveguide is fabricated with LPD method and its transmission characteristic for delivery of CO_2 lasers are experimented. Thermal effects of this kind of waveguide transmitting CO_2 lasers are theoretically simulated and measured. The fiber's output beam divergence angle and power profile are also studied to support the analysis of its thermal effects.

2 Experimental

The fabrication procedure is based on our reported LPD method [9]. A NiCr capillary tube was used as the substrate tube, length 1.5 m and bore size 1.5 mm. We designed and fabricated metal capillary tubes together with our partner metal capillary company. The fabrication (metal cold-drawn processing) and polishing procedures have influences on the roughness of NiCr tubing. The inner surface of the NiCr tube

was polished using a mechanochemical polishing method in the company. NiCr alloy tube has a complex elemental composition. A complex chemical solution was used to polish the inner wall of NiCr tubing. By optimizing both the fabrication and polishing procedures, the company provided NiCr tubing with inner surface roughness around 0.8 μm for this research. The roughness is acceptable for establishment of a long-wavelength (10.6 μm) infrared hollow waveguide. GeO_2 powder was dissolved in aqueous ammonia (3 wt%) to obtain a transparent GeO_2 precursor solution (7 wt%). The pH value of the solution was adjusted to 2 using diluted sulphuric acid. The solution was then injected into the NiCr capillary tube through a peristaltic pump (Lead Fluid BT100L) and the two ends of the tube were sealed using thermoplastics. The tube was inserted into a rotating sleeve (10 min/r) on a support device. GeO_2 solutes can be fully deposited on the inner tube wall in 7 days. In this work, a 1.5-m sample NiCr GeO_2 ATR hollow waveguide was prepared with two LPD cycles. The sample was then dried in air at 100 °C for 3 h. A 11 cm sample and a 60 cm sample were cut from the prepared 1.5-m sample for use in Fourier transform infrared spectrometer (FTIR) and transmission loss measurement, respectively.

Thermogravimetric analysis [STA449F3 (TGA/DSC)] were carried out to evaluate metal materials' resistance to thermal oxidation. Short copper, nickel, SUS, NiCr tubes were cut down, split and flatten to small sample pieces. These samples were heated in air atmosphere, with the temperature rising to 1100 °C at the speed of 20 °C/min (The melting point of GeO_2 is 1115 °C). The Fourier transform infrared spectroscopy (FTIR) absorbance spectra were taken with a FTIR spectrometer (FTIR, Bruker 80V) using an external beam and an off-axis parabolic gold mirror to focus light into the hollow fiber (focal length 18 cm, spot size 1 mm). The core size and length of the samples used in FTIR analysis are 1.5 mm and 11 cm, respectively. A 60-cm-long waveguide sample cut from the fabricated 1.5 m NiCr hollow waveguide sample was used to transmit 6, 20 and 30 W CO_2 laser beam generated from a Coherent C30A laser device. A ZnSe convex lens, focal length of 100 mm, was used to focus the laser beam into fiber samples. A power detector (LP-3C) was used to measure the output beam power. Straight transmission losses of the NiCr hollow waveguide sample transmitting 6, 20 and 30 W CO_2 laser beam were acquired by cutback method. Temperature distribution of the sample's outer surface (the sample transmitting a 30-W CO_2 laser) was measured by a thermocouple thermometers (TES 1310K). The power detector was used during the measurement to monitor the output power as an indicator of transmission status change. The full divergence angel (FDA) of the output laser beam was measured by moving the beam profiler along the light path and records the beam width at each distance. To compare the thermal oxidation resistance

of a SUS-based GeO$_2$ ATR hollow fiber and a NiCr-based GeO$_2$ ATR hollow fiber, a 6-W laser was delivered directly onto the fibers' wall at the fiber input cross-section for 20 and 60 s. The transmission attenuation of the two guides and their attenuations after 20 and 60 s radiation were measured transmitting a 6-W CO$_2$ laser in normal working condition.

3 Results and discussion

Result of the thermogravimetric analysis (TGA) is given in Fig. 1. Copper, nickel, stainless steel and NiCr samples were heated in TGA device in air atmosphere with the temperature rising at the speed of 20 °C/min. The temperature gravity curve can be used to interpret the material's thermal oxidation resistance. Additional weight of the metal material indicates the beginning of thermal oxidation. Copper was the first to exhibit weight rise behavior among these materials at 600 °C. Severe mass change was then observed on the SUS sample after 700 °C. With the temperature rising to 1100 °C, the Ni sample has minor weight rise. As for NiCr sample, a weight loss behavior was discovered in heating process. We consider this may be caused by moisture or other attachments on the sample being incinerated. Hence, when temperature rises from room temperature to 1100 °C, NiCr sample suffers almost no thermal oxidation. This confirms that NiCr has a good intrinsic resistance to thermal oxidation. Compared with NiCr capillary tubes, the strength of the Ni capillary tubes degenerates after heat treatment; this may affect its use in practical applications. Thus, NiCr capillary tube is a good candidate as the structural tube for metallic GeO$_2$ ATR hollow fiber with improved high power transmission performance. Thermogravimetric analysis discloses the NiCr GeO$_2$ hollow waveguide can be potentially used at a temperature up to 1100 °C. The waveguide may

survive when heated by a high power laser beam within a short time (for example, misalignment occurs occasionally in the launching case), but waveguide damage is possibly caused by heat treatment at 1100 °C for a longer time. To solve this problem, water cooling jacket around the waveguide is recommended. Considering that the metallic tube is much thermally conductive, a water cooling jacket will be efficient to cool the waveguide in practical use.

Figure 2 gives the FTIR absorbance spectra of NiCr GeO$_2$ ATR hollow waveguide and NiCr substrate tube. The FTIR absorbance spectrum is mainly used to observe the low loss window shape and location of a hollow fiber. The unit of the absorbance in the FTIR spectrum can be written in a simple form as a. u. (absorbance unit) [15]. A low loss window can be observed in the absorbance spectrum of NiCr ATR hollow waveguide. No such low loss window was observed in the spectrum of NiCr substrate tube. The low loss window is located at the wavelength range from 9.7 to 11.7 μm, which is the same as the abnormal dispersion region of GeO$_2$. The appearance of the low loss window is originated from the GeO$_2$ film deposited by LPD method. An ATR structure for CO$_2$ laser transmission can be established by the GeO$_2$ film ($n_r < 1$ at wavelength 10.6 μm) and the air core inside the NiCr waveguide.

The measured attenuations of the NiCr GeO$_2$ ATR hollow waveguide transmitting 6, 20, 30 W CO$_2$ laser were 0.25, 0.38, 0.42 dB/m, respectively. The length of the waveguide sample for CO$_2$ laser transmission loss test is 60 cm. The theoretical straight loss for the HE$_{11}$ mode was calculated to be 0.029 dB/m using the classic Marcatili and Schmeltzer (MS) equation [see Eq. (1)]. Where α_{nm} is the attenuation coefficient, r is the waveguide bore radius, U_{nm} is a modal constant and N is the complex index of refraction. For the HE$_{11}$ mode, U_{nm} equals to 2.405. At the wavelength
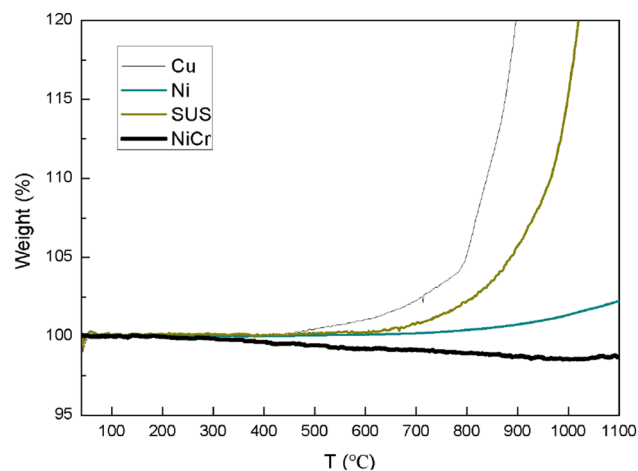

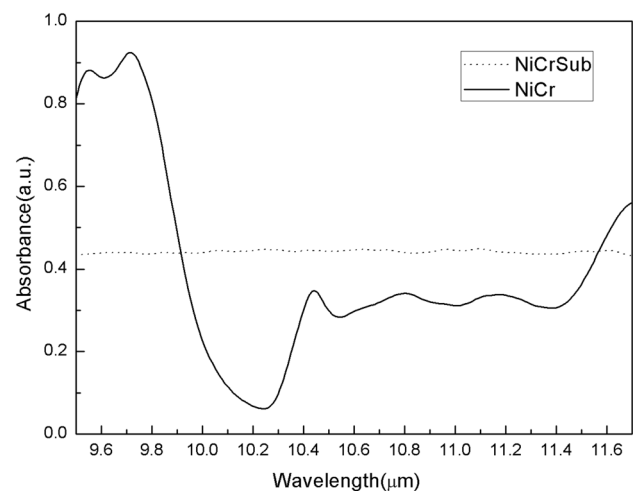**Fig. 1** Thermogravimetric analysis result of NiCr, Cu, Ni, SUS tubes

Fig. 2 Absorbance spectra for NiCr substrate tube and NiCr ATR GeO$_2$ hollow waveguide fabricated by two LPD cycles

of 10.6 μm, complex refractive index N of the GeO_2 film is 0.48–0.66j. The calculated result is lower than the measured loss. The sample tends to be bent by gravity on the supporting rail due to thin wall thickness (0.05 mm). The fiber sample was inserted into a glass tube to prevent it from bending when measuring straight loss with low input power (6 W). When higher input power applied, the glass tube was removed considering the glass tube may limit the waveguide from cooling. The sample waveguide was not perfectly straight without the glass tube and the heat induced by power loss enhanced its tendency to bending. This is why attenuation of the NiCr GeO_2 ATR hollow waveguide transmitting 20 and 30 W CO_2 laser is higher than the attenuation when 6 W input laser was applied. The calculation of theoretical loss assumes only the lowest-order HE_{11} mode exists in the hollow waveguide. Higher modes attenuate faster in a hollow fiber [16]. The hollow waveguide is capable of filtering higher order mode and achieve single-mode transmission if the bore size is sufficiently small [17]. When the bore size exceeds about 20 times the wavelength of operation, a metal/dielectric hollow waveguide tends to exhibit a multimodal transmission behavior [18]. In terms of the 1.5-mm bore ATR GeO_2 hollow fiber sample, the bore size is quite large. Higher order modes exist inevitably and cause the measured attenuations higher than the calculated result.

$$\alpha_{nm}(r) = \left(\frac{U_{nm}}{2\pi}\right)^2 \frac{\lambda^2}{r^3} Re\left[\frac{N^2 + 1}{2(N^2 - 1)^{\frac{1}{2}}}\right]. \tag{1}$$

In practical applications such as laser surgery, attention is also given to the output beam profile. It is desirable to maintain the spatial purity of the input laser beam since efficient cutting or ablation can be achieved with a small spot size. Figure 3 gives typical two-dimensional (2D) (a) and three-dimensional (3D) (b) output beam profiles of a straight NiCr GeO_2 ATR hollow fiber. As previously mentioned, the bore size of a hollow fiber has influence on the transmission modes the fiber supports. The as-fabricated NiCr GeO_2 ATR hollow fiber theoretically supports high-order modes. The Gaussian-like beam profile indicates that the lowest-order
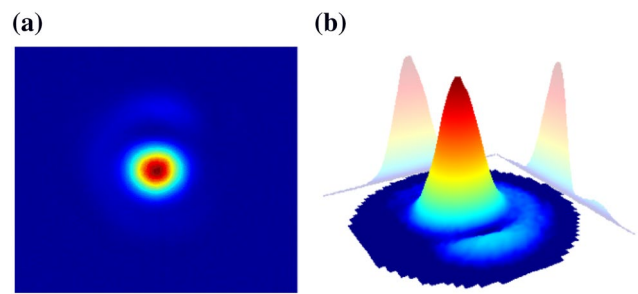
(a)   **(b)**

Fig. 3 Two-dimensional (2D) (**a**) and three-dimensional (3D) (**b**) output beam profiles of a straight NiCr GeO_2 ATR hollow fiber

HE_{11} mode is the dominant mode in the NiCr fiber. However, the shape of the 2D profile is not strictly a circle and there exists an outer ring. These confirm that higher order mode transmission exists in the waveguide. Multi-mode transmission has caused higher attenuation of the fiber than theoretical calculation.

For a portion of a cylindrical waveguide, the lost power per unit length P_1 (L) is transformed into two thermal flows, Q_{cv} (L) along the waveguide due to conduction and Q_{cd} (L) outward due to convection [19, 20]. A thermal equilibrium can be obtained as Q_{cd} (L) + $\Delta L P_1$ (L) = Q_{cv} (L) + $Q_{cd}(L + \Delta L)$. Based on this thermal equilibrium model and electro-magnetic wave theory, Miyagi et al. carried out an method to simulate the temperature distribution along an operating leaky hollow waveguides as given in the following equations:

$$T_{tr}(z) = T_{\infty} + \frac{2P_0}{kS} \sum_{n=1}^{N} \frac{\alpha_n \eta_n}{q^2 - 4\alpha_n^2} \exp\left(-2\alpha_n z\right) + c_1 \exp\left(qz\right) + c_2 \exp\left(-qz\right) + T_{os}(z), \tag{2}$$

$$T_{os}(z) = \frac{1}{2kS} \sum_{\substack{n, m \\ n \neq m}}^{N} \frac{|I_{nm}| \cos\left(U_{nm} z - \theta_{nm} - \delta_{nm}\right) \cdot \exp\left[-(\alpha_n + \alpha_m)z\right]}{\left[(\alpha_n + \alpha_m + q)^2 + U_{nm}^2\right]^{\frac{1}{2}} \cdot \left[(\alpha_n + \alpha_m - q)^2 + U_{nm}^2\right]^{\frac{1}{2}}}, \tag{3}$$

where T and T_{∞} are the waveguide surface temperature and room temperature, respectively. S is the wall thickness of the waveguide and s is the length of the periphery of the waveguide. $q = \sqrt{(hs/kS)}$, where k and h are the heat conductivity of the waveguide wall and the heat transmission of air, respectively, P_0 is the input power of CO_2 laser, η_n is the coupling coefficient of the nth mode from the indent beam, α_n, α_m is the attenuation constants of CO_2 laser transmitting in the hollow fiber, and c_1, c_2 are two constants determined by the boundary conditions at the input and output ends. Take structural and transmission mechanism differences
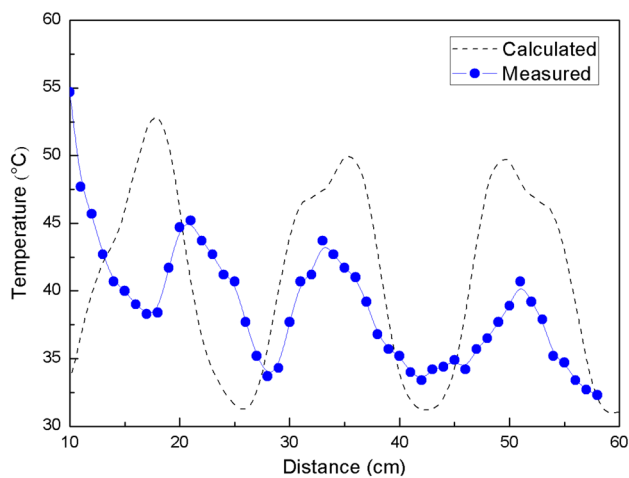
Fig. 4 Theoretically calculated (dash) and measured (solid) temperature distribution along the axis of NiCr hollow waveguide transmitting a 30-W CO₂ laser (calculated result without consideration of coupling loss)

Fig. 5 Predicted maximum input laser powers and the corresponding fiber temperature distribution for given $T_{max} = 1100$ °C

between leaky and ATR hollow fiber into account, the fiber temperature of the metallic ATR hollow fiber can be simulated [21].

Equations (2) and (3) does not include the influence the coupling loss. However, the influence of coupling loss dissipates quickly in a short distance. The simulated temperature distribution can represent the temperature distribution of the part of fiber without the influence of coupling loss. On the other hand, a cooling device is often used at the input end of the hollow fiber leaving the rest of the fiber cooled by natural air convection in practical applications. The theoretical temperature distribution is an important reference to establish a maximum input power for the hollow fiber. The theoretical temperature distribution of the NiCr-based ATR fiber sample (length 60 cm, bore size 1.5 mm) transmitting 30 W CO₂ laser is simulated (Fig. 4). Measured temperature distribution along the sample fiber axis is also shown in Fig. 4. An oscillatory distribution of fiber temperature is observed. As we discussed, the fiber sample is able to support multi-mode transmission and multi-mode behavior is observed through beam profile. This oscillatory distribution is caused by the interference of the different laser transmission modes. The measured temperature distribution is in the temperature range as theoretically simulated (measured 32–47, simulated 31–52). By applying a maximum temperature, the simulated temperature range can be used to predict the maximum power this hollow waveguide can carry. As for the NiCr GeO₂ ATR hollow waveguide, if we set the maximum temperature rise to be 1100 °C, the waveguide can hold up to 1078 W with nature air convection according to calculation (Fig. 5).

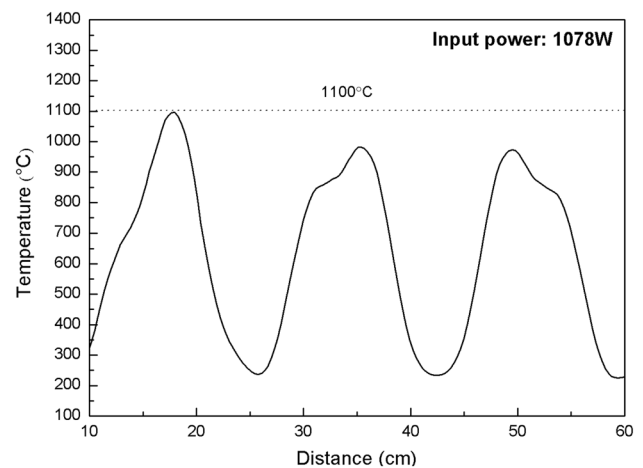The temperature distribution of the overall hollow fiber is caused by two distinct effects: coupling loss and the continuous transmission loss. Equations (2) and (3) offer a theoretical way to simulate the temperature distribution originated from only transmission loss. The coupling is more sensitive to launch alignment [20]. A fraction of the laser input power is lost in short distance due to coupling loss. The lost power is transformed to heat and being conducted along the fiber, forming a parallel temperature distribution. Misalignment may induce substantial temperature rise at the input end of the waveguide. Assuming the lost, laser power due to coupling was absorbed by the front-end cross-section of the fiber, this temperature distribution induced by coupling loss can be shown as in the following equations:

$$T_{cp} = \frac{W}{msk} \exp\left(-ml\right), \tag{4}$$

$$T = T_{tr} + T_{cp}, \tag{5}$$

where W is the power absorbed by the front end, s is the cross-sectional area, k is the heat conductivity of the waveguide, l is the distance from the front end, and $m = (4h/k) \cdot D_2 / (D_2^2 - D_1^2)$, where D_2 is the outside diameter, and D_1 is the inside diameter of the fiber [20].

The overall temperature distribution includes both the influence of coupling and transmission losses as in Eq. (5). The actual power loss at the front end is hart to quantitatively determine, because the absolute beam intensity profile and the absorption characteristics of the fiber entrance face are unknown. After measuring transmission loss and temperature distribution, the test sample was cut at 10 cm of the front end. With the same input power and launching condition, the output power of this 10 cm sample was measured. Because the coupling loss is much higher than the transmission loss of the fiber, especially at the front end of the fiber, we assumed that the difference between input
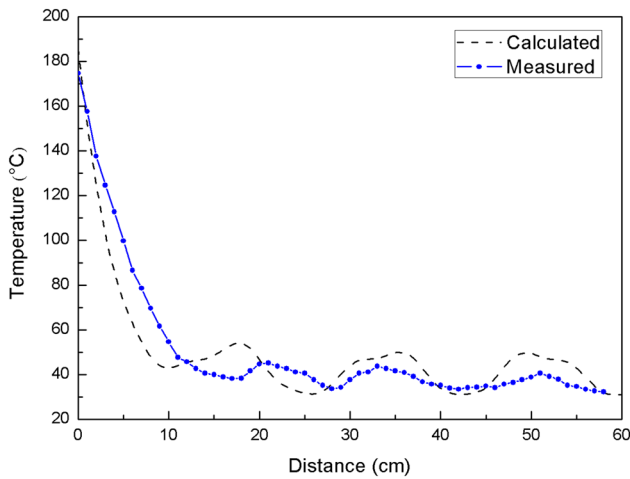
Fig. 6 Theoretically calculated (dash) and measured (solid) temperature distribution along the axis of NiCr hollow waveguide transmitting a 30 W CO_2 laser (calculated result considered both transmission and coupling losses)

power and output power of this 10 cm sample was absorbed by the front end. In this case, it could be learnt that power absorbed by the front end is almost 3 W (in 10 cm, input power 30 W). Assuming the 3 W laser power is all lost at the front-end cross-section, the overall temperature distribution can be calculated with Eq. (5). In Fig. 6, the theoretical temperature distribution taking account of both coupling loss and power attenuation is given and compared with the measured temperature distribution. The adjusted theoretical result mostly matched the measured temperature distribution, including the influence of the coupling loss. It can be used as a reference in deciding the cooling condition in practical applications.
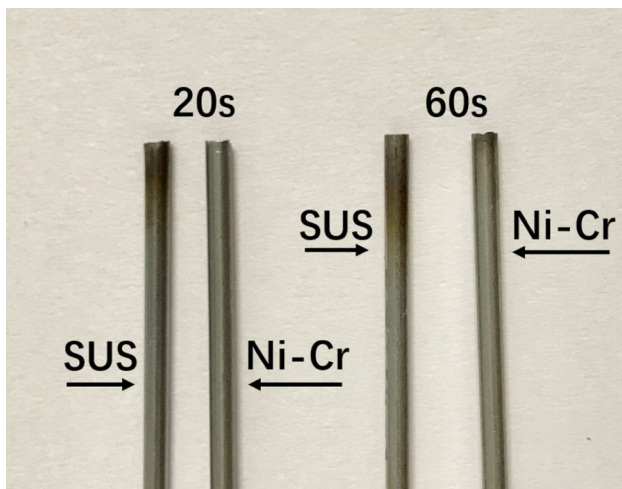

Fig. 7 Digital picture of SUS and NiCr ATR fibers under direct irradiation of 6 W CO_2 laser for 20 and 60 s

As we discussed above, the coupling loss is sensitive to launch alignment. The overall temperature distribution calculated in Fig. 6 is based on a properly aligned transmission system. If misalignment occurs, laser is directly delivered onto fiber inner wall, temperature could rise even higher. In practical applications, misalignment may happen during calibration and other accidents. For some metallic capillary tube GeO_2 ATR waveguides that are sensitive to thermal oxidation, the temperature rise could do unrecoverable damage to the waveguide in very short time. Figure 7 shows the digital picture of SUS and NiCr ATR fibers under direct irradiation of 6 W CO_2 laser for 20 and 60 s. In this experiment, a 6-W laser beam was directly radiates onto the cross-section of the waveguide input end to simulate extreme conditions such as misalignment of laser to waveguide. From the photos of laser heating and damage one can see that the NiCr waveguide can withhold longer in extreme temperatures compared with the SUS waveguide. In optical transmission systems, the fiber inevitably does not always operate under optimum coupling or aligned launching conditions. In these conditions, the temperature of the input end of hollow wavegudie could rise far higher than normal working condition. The laser delivery system may be damaged, which possiblly casues some serious accidents. The thermal oxidation resistance of NiCr alloy makes the NiCr waveguide take longer before real damage done to the waveguide, giving researchers or operators enough time to stop the device and reduce further damage. Under a normal working condition, the input end of the NiCr waveguide remains almost intact after transmiting a 6-W CO_2 laser beam for more than 30 min.

To investigate the damage the GeO_2 film is possibly suffered under the simulated misalignment condition, the radiated waveguide samples shown in Fig. 7 were used to transmit a 6-W CO_2 laser under a normal working condition. If the GeO_2 film at the input end of the waveguide has already been damaged, the transimission properties would deteriorate. The original attenuation (before radiated) of
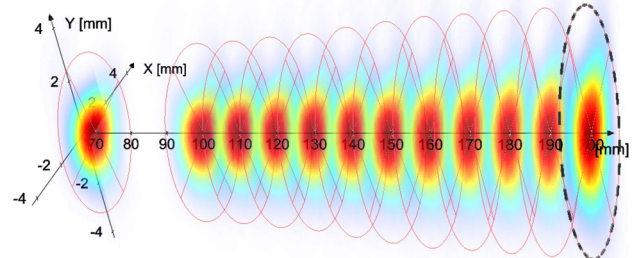

Fig. 8 The divergence angle fitted based on the output beam width and distance

NiCr ATR hollow waveguide is 0.26 dB/m, and attenuations after 20 and 60 s radiation are 0.26 and 0.59 dB/m, respectively. For SUS ATR hollow waveguide, the original attenuation and attenuations after 20 and 60 s radiation are 0.27, 0.62 and 0.77 dB/m, respectively. It is clear that in the simulated extreme working condition, the GeO$_2$ film inside the input end of the NiCr waveguide could remain intact within 20 s, and undergo somewhat damage within 20–60 s. The GeO$_2$ film inside the input end of the SUS wavegudie was suffered greater damage during this period.

Figure 8 gives the measured output beam profiles along the light path of a NiCr ATR hollow waveguide at different distances (delivering a 6 W CO$_2$ laser). The full divergence angle was fitted based on the output beam width and distance data. The output laser beam of a straight waveguide sample has a FDA of about 22 mrad. This FDA is quite small and desirable in applications. In practical use, a focal convex is often used at the output end of a hollow fiber to enhance the power density of the output laser beam. FDA is a crucial parameter when choosing an appropriate focal convex. For a hollow fiber with a small bore size, a small FDA means that no additional focal convex is required to enhance the power density.

4 Conclusion

GeO$_2$ film deposited on different materials exhibit different transmission characteristics. New materials should be investigated for construction of GeO$_2$ ATR hollow waveguide. NiCr is often used in thermocouple heater. TGA manifests that the NiCr could withhold thermal oxidation resistance at least up to 1100 °C. NiCr capillary tubes were chosen to complement the disadvantage of metallic tubes that they prone to be oxidized in high temperature in material point of view. NiCr capillary tube GeO$_2$ ATR hollow fiber was fabricated by LPD process. Straight transmission loss is measured to be 0.25, 0.38, and 0.42 when transmitting 6, 10 and 30 W laser, respectively. Take structural and transmission mechanism differences between leaky and ATR hollow fiber into account, a method to simulate the fiber temperature distribution was carried out based on the work of Miyaki et al. The influence of the coupling loss on the temperature distribution is also theoretically and experimentally investigated. The stimulation can properly predict the temperature range of the measured results. Thus, when a maximum temperature is applied, a theoretically maximum input power could be obtained. To simulate an extreme misalignment condition, the NiCr-based fiber and SUS-based fiber were irradiated directly by a 6-W CO$_2$ laser. Result shows that NiCr fiber has better resistance to thermal oxidation and less likely to be damaged by misalignment. The fiber's output beam divergence angle and power profile are also studied to support

the analysis of its thermal effects. In conclusion, the NiCr capillary tube GeO$_2$ ATR hollow fiber is a good candidate for construction of durable GeO$_2$ ATR hollow fiber in high power applications.

References

1. A. Hongo et al., Transmission of 1 kW-class CO$_2$ laser light through circular hollow waveguides for material processing. Appl. Phys. Lett. **58**(15), 1582–1584 (1991)
2. B. Temelkuran et al., Wavelength-scalable hollow optical fibres with large photonic bandgaps for CO$_2$ laser transmission. Nature **420**(6916), 650 (2002)
3. I. Shavrin et al., Gas refractometry using a hollow-core photonic bandgap fiber in a Mach–Zehnder-type interferometer. Appl. Phys. Lett. **100**(5), 4729 (2012)
4. C. Huang et al., Infrared hollow optical fiber probes for reflectance spectral imaging. Appl. Opt. **54**(14), 4602–4607 (2015)
5. C.C. Gregory, J.A. Harrington, Attenuation, modal, and polarization properties of n < 1, hollow dielectric waveguides. Appl. Opt. **32**(27), 5302–5309 (1993)
6. J. Liu, J. Han, X. Zhao, Study on Na$_2$O-GeO$_2$-SiO$_2$-PbO glasses used as the gladding materials of hollow waveguides for transmitting CO2 laser. J. Wuhan Univ. Technol. Mater. Sci. Ed. **4**, 48–54 (1996)
7. C. Jing, J. Hou, X. Xu, Fabrication and optical characteristics of thick GeO$_2$ sol–gel coatings. Opt. Mater. **30**(6), 857–864 (2008)
8. L. Hou et al., Polycrystalline germanium dioxide hollow-core fibers and their performance. Infrared Phys. Technol. **38**(3), 193–199 (1997)
9. C. Jing et al., Facile liquid phase deposition of thick reflective GeO$_2$, film for hollow waveguide delivery of CO$_2$, laser radiation. Appl. Phys. A **90**(2), 367–373 (2008)
10. C. Jing et al., Low-temperature, low-cost growth of robust ATR GeO$_2$ hollow fibers based on copper capillary tubes for transmission of CO$_2$ laser light. Proc SPIE **8938**(1), 393–398 (2014)
11. C. Jing et al., Metallic attenuated total reflection infrared hollow fibers for robust optical transmission systems. Appl. Phys. Lett. **105**(1), 011102–011102-4 (2014)
12. X. Wang et al., Preparation and transmission characteristics of a mid-infrared attenuated total reflection hollow waveguide based on a stainless steel capillary tube. Appl. Opt. **55**(23), 6404 (2016)
13. M. Miyagi, S. Karasawa, S. Nishida, Temperature distribution along oversized hollow-core waveguides for infrared radiation. Appl. Opt. **26**(21), 4581–4586 (1987)
14. X. Wang et al., Thermal behaviors of stainless steel tube based GeO$_2$, ATR hollow fibers for transmitting CO$_2$, laser radiations. Opt. Laser Technol. **95**, 42–45 (2017)
15. C.M. Bledt, D.V. Kopp, J.A. Harrington et al., in *Proc. SPIE 8218, Optical Fibers and Sensors for Medical Diagnostics and Treatment Applications XII*, p. 821802 (2012)
16. Y. Hiratani, M. Miyagi, S. Nishida, Power handling capability of dielectric-coated, metallic, hollow waveguides for CO$_2$, laser light. Opt. Laser Technol. **17**(3), 135–138 (1985)
17. Y. Matsuura, T. Abel, J.A. Harrington, Optical properties of small-bore hollow glass waveguides. Appl. Opt. **34**(30), 6842–6847 (1995)

18. C. Jing, W. Kendall, J.A. Harrington, A simple way to establish a dual-core hollow fiber for laser surgery applications. SPIE BiOS **9702**, 97020D (2016)

19. J. Ma, Y. Sun, B. Li, H. Chen, Spectral collocation method for radiative–conductive porous fin with temperature dependent properties. Energy Convers. Manag. **111**, 279 (2016)

20. Y.S. Sun, B.W. Li, Spectral collocation method for transient conduction-radiation heat transfer. J. Thermophys. Heat Transf. **24**(4), 823–832 (2012)

21. D. Su et al., Thermal effects in a hollow waveguide beam launch for CO_2 laser power delivery. Appl. Opt. **35**(24), 4787 (1996)